Effect of Order of Mixing on Morphology and Thermal Properties of the Compatibilized PBT and ABS Alloys/OMT Nanocomposites

Junfeng Xiao,[1,2,3] Yuan Hu,[1] Hongdian Lu,[1] Yibing Cai,[1] Zuyao Chen,[2] Weicheng Fan[1]

[1]*State Key Laboratory of Fire Science, University of Science and Technology of China, Hefei, 230026, Anhui, People's Republic of China*
[2]*Department of Chemistry, University of Science and Technology of China, Hefei, 230026, Anhui, People's Republic of China*
[3]*Department of Safety Engineering, Anhui Institute of Architecture and Industry, Hefei, 230022, Anhui, People's Republic of China*

Received 23 October 2005; accepted 17 January 2006
DOI 10.1002/app.24218
Published online in Wiley InterScience (www.interscience.wiley.com).

ABSTRACT: Poly(butylene terephthalate) (PBT) and acrylonitrile–butadiene–styrene terpolymers (ABS) alloys/organically modified montmorillonite (OMT) nanocomposites using terpolymers of random ethylene, methyl acrylate, and glycidyl methacrylate as the reactive compatibilizer were prepared by different melt-mixing sequences. The microstructures were characterized by scanning electron microscopy, X-ray diffraction, transmission electron microscopy, and high-resolution electron microscopy. It was found that order of mixing affects the dispersion state of OMT in the alloy matrix. The crystallization behavior of PBT in the compatibilized PBT and ABS alloys/OMT nanocomposites was studied by wide angle X-ray diffraction. It revealed that order of mixing has influence on the preferential crystal growing direction of PBT owing to the antagonistic effect of ABS and OMT. Thermogravimetric analyses and differential scanning calorimetry also showed order of mixing changes the thermal property of the compatibilized PBT and ABS alloys/OMT nanocomposites. © 2007 Wiley Periodicals, Inc. J Appl Polym Sci 104: 2130–2139, 2007

Key words: poly(butylene terephthalate); alloys; nanocomposites; XRD; TGA

INTRODUCTION

Poly(butylene terephthalate), PBT, is an important commercially available semicrystalline engineering thermoplastic with many valuable properties including a high rate of crystallization, good abrasion and chemical resistance, thermal stability, and excellent processing properties. However, pure PBT has low notched impact strength and heat distortion temperature. Many attempts have been made to improve the impact property of PBT through blending with an elastomeric modifier such as emulsion-made core-shell impact modifiers,[1,2] functionalized reactive rubbers,[3,4] and ethylene vinyl acetate copolymer.[5,6]

In the meanwhile, PBT was successfully toughened by acrylonitrile–butadiene–styrene terpolymers (ABS), although they themselves are an immiscible system.[7–24] The morphology and toughness of PBT/ABS blends have been thoroughly explored by Paul et al.[15,17–21] The factors that influence mechanical properties of PBT/ABS blends, especially notched fracture behavior, include ABS type and concentration, processing conditions, compatibilizer composition and content, PBT molecular weight, mixing sequence, and so on. Unfortunately, the existence of ABS often decreased other properties of PBT such as the tensile strength, modulus, and elongation at break.

In recent years, polymer/clay nanocomposites, as a very promising alternative to conventional filled polymers, have attracted considerable attention from academic and industrial researchers. The dispersion of these ultrathin (1 nm) ultrahigh surface-area clay layers (normally less than 10 wt %) within a polymer matrix leads to nanocomposites exhibiting markedly improved physicochemical properties, such as higher strength and modulus, better dimensional and thermal stabilities, higher heat distortion temperature, and chemical stability, as well as more efficient gas barrier properties and flame retardancy, than pure polymers or conventional microcomposites.[25,26] As a reinforced method, PBT/clay nanocomposites have been prepared by melt intercalation[27–30] or *in situ* intercalative polymerization.[31,32]

Correspondence to: Y. Hu (yuanhu@ustc.edu.cn).
Contract grant sponsor: China NKBRSF project; contract grant number: 2001CB409600.
Contract grant sponsor: National Natural Science Foundation of China; contract grant numbers: 50323005 and 50476026.

In the present work, the PBT/ABS/organically modified montmorillonite (OMT) nanocomposites using terpolymers of random ethylene, methyl acrylate, and glycidyl methacrylate (GMA) as the reactive compatibilizer were prepared by melt blending method. The effect of order of mixing on morphology of the compatibilized alloys nanocomposites was studied. The crystallization behavior and thermal properties of the nanocomposites were also investigated.

TABLE I
Compositions of the Compatibilized PBT/ABS/OMT Nanocomposites

Sample	Compositions
B0	PBT/EMG/ABS [65/5/30 wt %]
B1	PBT/EMG/ABS/OMT [62/5/30/3 wt %]
B2	(PBT/EMG/OMT)/ABS [(62/5/3)/30 wt %]
B3	PBT/EMG/(ABS/OMT) [62/5/(30/3) wt %]
B4	(PBT/EMG/ABS)/OMT [(62/5/30)/3 wt %]

EXPERIMENTAL

Materials

PBT (PBT1084, density = 1.31 ± 0.02, intrinsic viscosity = 0.84 ± 0.02) used in this study was obtained as pellets from Nantong Xingchen Synthetic Material, China. ABS (PA-727) was supplied as pellets by Qimei Stock Company, Taiwan. The reactive compatibilizer, random ethylene/methyl acrylate (MA)/GMA terpolymers (EMG) (LOTADER®, AX8900), was received from ATOFINA, France. The content of GMA and MA in EMG, respectively, is 8 wt % and 24 wt %. OMT was prepared from Na-montmorillonite (with a cation exchange capacity of 122 meq/100 g) by ion exchange reaction using cetyl pyridium chloride in water according to the reported method.[30]

Preparation of the compatibilized PBT and ABS alloys/OMT nanocomposites

The OMT and PBT pellets were dried under vacuum at 80°C for at least 10 h, and ABS pellets was dried for 4 h in a circulating air oven at 80°C before use, whereas the compatibilizer was used as received. The blend components were melt mixed in a twin-roll mill (XK-160, made in Jiangsu, China) with the roll speed of 100 rpm at 230°C. Four different mixing procedures were used to prepare the compatibilized PBT and ABS alloys/OMT nanocomposites with the same compositions containing of 3 wt % OMT, 5 wt % the compatibilizer EMG, and 30 wt % ABS. Four different mixing sequences were as follows: to mix PBT, EMG, ABS with OMT in a single step (B1); to mix PBT and EMG with OMT first and then blend the PBT/EMG/OMT nanocomposite with ABS (B2); first to prepare the ABS/OMT nanocomposite and then mix it with PBT and EMG (B3); to prepare the PBT/EMG/ABS blend first and then mix the blend with OMT (B4). The samples are identified in Table I. For comparison, the blend B0 containing 5 wt % EMG and 30 wt % ABS was melt mixed with PBT in one step.

Characterization

X-ray diffraction (XRD) experiments were performed at room temperature on a Japan Rigaku D/max-rA X-ray diffractometer (30 kV, 10 mA) with Cu Kα (λ = 1.54, 178 Å) irradiation at the rate of 2°/min in the range of 1.5–10 ° or 5–40°.

The morphologies of the fractured surfaces of the samples were examined by scanning electron microscopy (SEM) using the XT30 ESEM-TMP apparatus operating at an accelerating voltage of 15 KV. The samples were taken from the impact broken pieces. The fracture surfaces of the broken pieces were coated with gold to enhance the conductivity before the SEM study.

Transmission electron microscopy (TEM) images were obtained on a JEOL JEM-100SX microscope with an acceleration voltage of 100 kV. High-resolution electron microscopy (HREM) images were obtained by JEOL 2010 with an acceleration voltage of 200 kV. TEM and HREM specimens were cut from epoxy blocks with the nanocomposites powders embedded, at room temperature using an ultramicrotome (Ultracut-1, UK) with a diamond knife. Thin specimens, 50–80 nm, were collected in a trough filled with water and placed on 200 mesh copper grids.

Thermogravimetric analyses (TGA) were carried out using a Netzch STA-409c thermal analyzer under nitrogen flow at the rate of 10°C/min.

Differential scanning calorimetry (DSC) was carried out on a Perkin–Elmer DSC7 under continuous nitrogen flow. DSC was calibrated using an Indium standard (melting temperature T_m = 156.4°C and enthalpy of fusion ΔH = 288.4 J/g). The samples were first heated from 0 to 250°C at a rate of 20°C/min, maintained for 1 min to remove thermal history, and cooled at a rate of 20°C/min to 0°C. After 1 min, the cooled samples were then reheated at a rate of 20°C/min to 250°C. The glass transition temperature (T_g) values were defined at the midpoint of the specific heat steps while the melting temperature (T_m) and crystallization temperature (T_c) were defined at the maxima of the DSC peaks. The corresponding enthalpy changes, ΔH_m and ΔH_c were obtained from peak area integration. The weight percentage crystallinity of PBT was calculated using 142 J/g as the melting enthalpy for 100% crystallized PBT.[33]

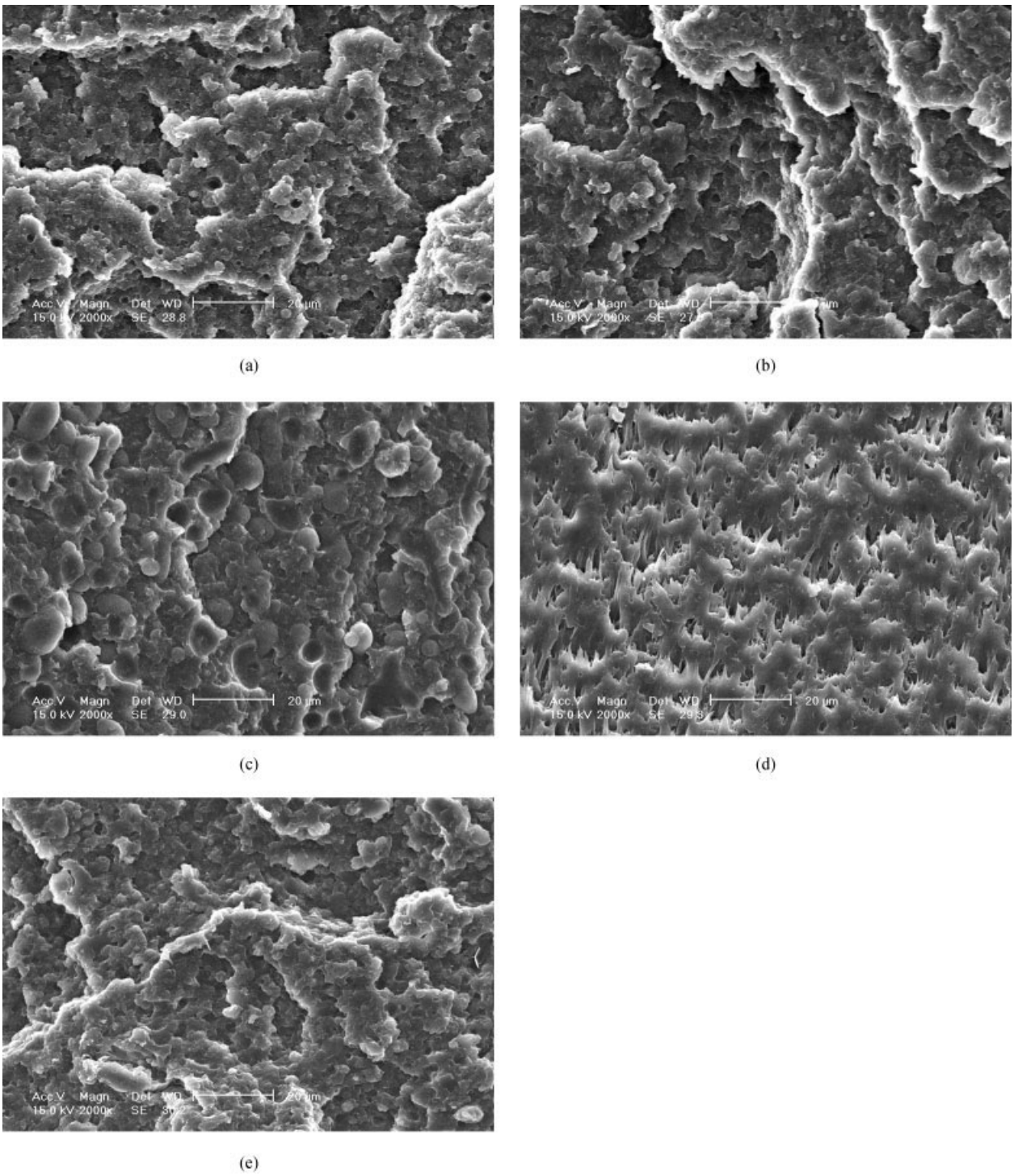

Figure 1 SEM images of fracture surfaces of (a) B0: [PBT/ABS/EMG], (b) B1: [PBT/ABS/EMG/OMT], (c) B2: [(PBT/EMG/OMT)/ABS], (d) B3: [PBT/EMG/(ABS/OMT)], (e) B4 [(PBT/ABS/EMG)/OMT].

RESULTS AND DISCUSSION

Morphology of the compatibilized PBT and ABS alloys/OMT nanocomposites

The microstructure and morphology of polymer/clay nanocomposites are typically elucidated by SEM, XRD, TEM, and HREM. Figure 1 shows SEM images of the fractured surfaces of the blends. The sample B0 [PBT/ABS/EMG blend] [Fig. 1(a)] shows ABS particles uniformly dispersed within the PBT matrix. It indicated the compatibilizer EMG increased the interfacial adhesion between the ABS and PBT phases. It is because these acrylic terpolymers were miscible with the styrene–acrylonitrile phase of ABS, whereas the

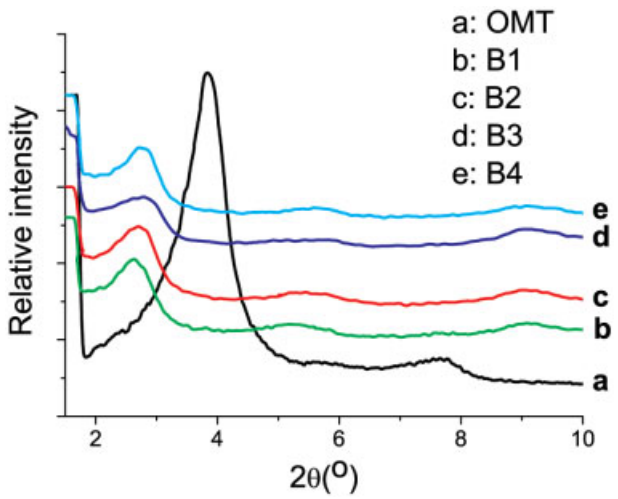

Figure 2 XRD patterns of (a) OMT, (b) B1, (c) B2, (d) B3, and (e) B4. [Color figure can be viewed in the online issue, which is available at www.interscience.wiley.com.]

epoxide groups of the GMA repeat units could react with the carboxyl or hydroxyl endgroups of PBT during melt processing to form an *in situ* graft copolymer at the PBT/ABS interface.[17,24] After OMT was added into the compatibilized PBT and ABS alloys, SEM images [Figs. 1(b)–1(e)] show the fracture surfaces became smoother than B0 and order of mixing changed the morphology. When all of the components were mixed together in a single-step (sample B1 [PBT/EMG/ABS/OMT], see Table I), Figure 1(b) shows a decrease in ABS particle size, compared with B0. It may be that the clay transferred the interfaces acting as an active interfacial modifier.[34] Figure 1(c) represents SEM image of B2 [(PBT/EMG/OMT) /ABS], where PBT, EMG, and OMT were first melt mixed together and then ABS was added into the PBT/EMG/OMT nanocomposite. It shows that the particle size became large and regular, which reveals a decrease of the compatibility. It may be attributed to the microstructure of the alloy. EMG intercalated into the layers of OMT and ABS not so that OMT reduced the interconnecting of the compatibilizer EMG and ABS, which need the confirmation of XRD and TEM. For B3 [PBT/EMG/ (ABS/OMT)], ABS and OMT was first melt mixed together and then was blended PBT and EMG. Figure 1(d) shows that the compatibility increases so that the fracture surface became ductile and ABS phase was not distinguishable. For B4 [(PBT/ABS/EMG) /OMT] where OMT was mixed with the PBT/ABS/EMG blend, Figure 1(e) shows the morphology of fracture surface was similar to that of B0.

Figure 2 shows the XRD patterns of the compatibilized PBT and ABS alloys/OMT nanocomposites prepared by different mixing procedures as well as the XRD pattern of OMT. The peaks correspond to the plane (001) reflections of the clay. The d_{001} peak of

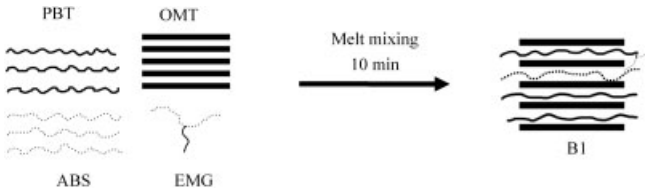

Figure 3 Schematic illustration for preparation of the nanocomposites B1.

OMT observed at $2\theta = 3.71°$ corresponds to 2.38 nm interlayer spacing [Fig. 2(a)]. After OMT was combined with the compatibilized PBT and ABS alloys via different blending sequence, it shows that the peaks shift obviously to lower angles and the mixing sequences influence the dispersion of OMT in the polymer matrix.

When all of the components were mixed together in a single step (B1), the XRD result [Fig. 2(b)] shows the peak at $2\theta = 2.68°$ corresponds to 3.30 nm, indicating the formation of the intercalated structure. It may reveal that either or both of the PBT and ABS chains have intercalated into the clay layers. Figure 3 shows the scheme of preparation of B1. A two-step melt-blending approach was, respectively, employed for sample B2, B3, and B4. For B2, PBT, EMG, and OMT were first melt mixed together and then ABS was added into the PBT/EMG/OMT nanocomposite. The XRD profile of PBT/EMG/OMT nanocomposite is shown in Figure 4. And the XRD patterns of OMT and B2 were also presented only for comparison. The peak at 2.70° corresponding to 3.28 nm [Fig. 4(b)] suggests the intercalated morphology of the PBT/EMG/OMT nanocomposite. After blending with ABS, there is little difference in the location of the peak [Figs. 2(c) or 4(c)]. It indicates no further intercalation occurring during

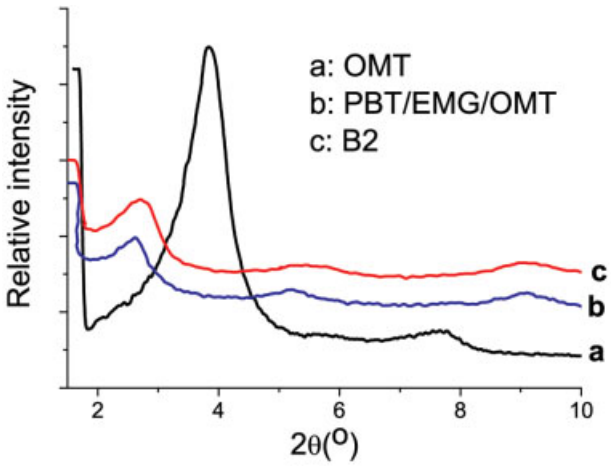

Figure 4 XRD patterns of (a) OMT, (b) the PBT/EMG/OMT nanocomposite, and (c) its blend with ABS, B2. [Color figure can be viewed in the online issue, which is available at www.interscience.wiley.com.]

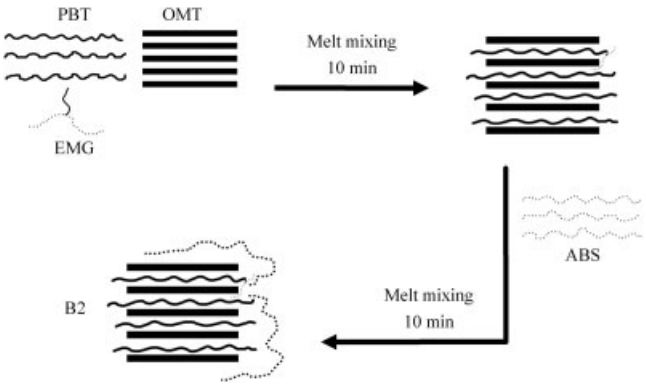

Figure 5 Schematic illustration of the nanocomposites B2 synthesis.

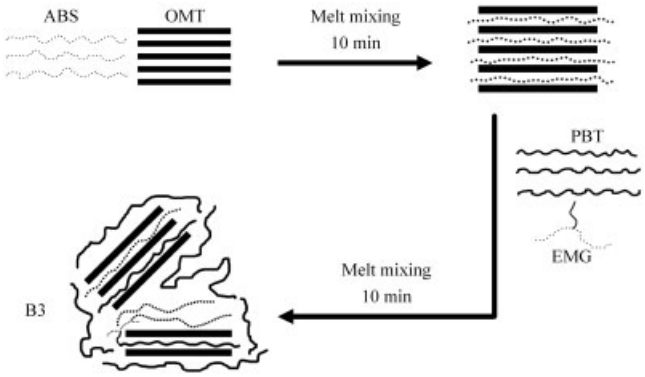

Figure 7 Schematic illustration for preparation of the nanocomposites B3.

the second-step mixing and the clay layers were kept in the PBT matrix from migrating to the dispersed ABS phase, which confirmed the SEM analysis. This may be due to the more favorable interactions such as the polar interactions between OMT and the carboxyl or hydroxyl groups on the PBT backbone than those of OMT and ABS.[27] Figure 5 presents the schematic illustration for preparation of B2. A two-step procedure where ABS and OMT was first melt mixed together before adding PBT and EMG in a second blending was applied to B3. Figure 6 presents the XRD patterns of the ABS/OMT nanocomposite and its blend B3. A sharp diffraction peak at 2.79° [Fig. 6(b)] appears in the ABS/OMT nanocomposite, indicating ABS intercalating into the clay layers. However, in B3 [Figs. 2(d) or 6(c)], the peaks continue shifting to lower angle and show a very broadened and weak peak around 2.69°. It exhibits partially exfoliated, partially intercalated structure in B3. The reason may be that PBT intercalate into the clay layers during the second melt mixing, leading to the increase of the spacing distance. The theoretical model of B3 is illustrated in Figure 7. For B4 where the PBT/EMG/ABS blend was first prepared and then mixed with OMT, the XRD peak at 2.70° [Fig. 2(e)] resembles that of B1, showing the formation of the intercalated structure. The scheme for B4 is illustrated in Figure 8.

To further confirm the dispersion state of the clay layers and the morphology of the alloys, the TEM and HREM observations were carried out. Figures 9 and 10, respectively, show the TEM and HREM images of the compatibilized PBT and ABS alloys/OMT nanocomposites prepared by different mixing sequences. In the TEM photograph, the gray continuous region corresponds to PBT phase and the ABS phases appear as dark domains. The black lines correspond to the clay layers. The TEM image of B1 in a low magnification [Fig. 9(a)] shows clearly the two-phase morphology with large and coarse ABS domains dispersed in PBT matrix, and the clay dispersed both in PBT and ABS phases, but mostly in PBT and near the interfacial area. It may be that the clay acts as an active interfacial modifier to decrease the interfacial energy.[34] In contrast to B1, the TEM

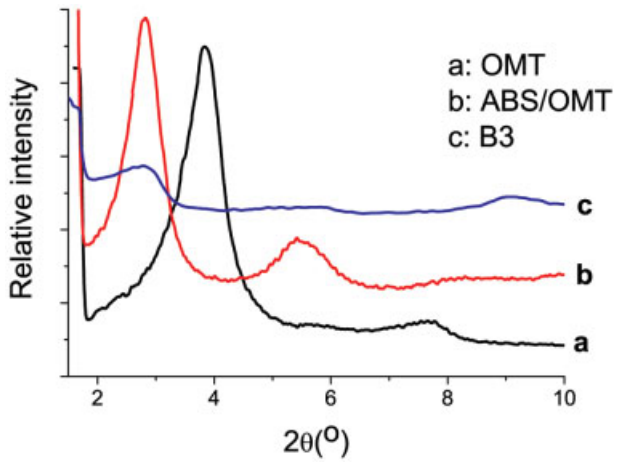

Figure 6 XRD patterns of (a) OMT, (b) the ABS/OMT nanocomposite, and (c) B3. [Color figure can be viewed in the online issue, which is available at www.interscience.wiley.com.]

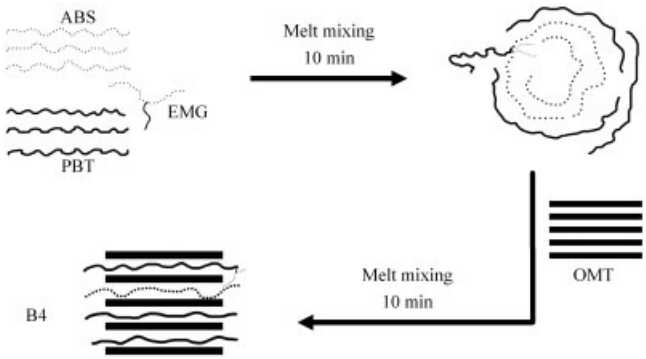

Figure 8 Schematic representation of preparation of the nanocomposites B4.

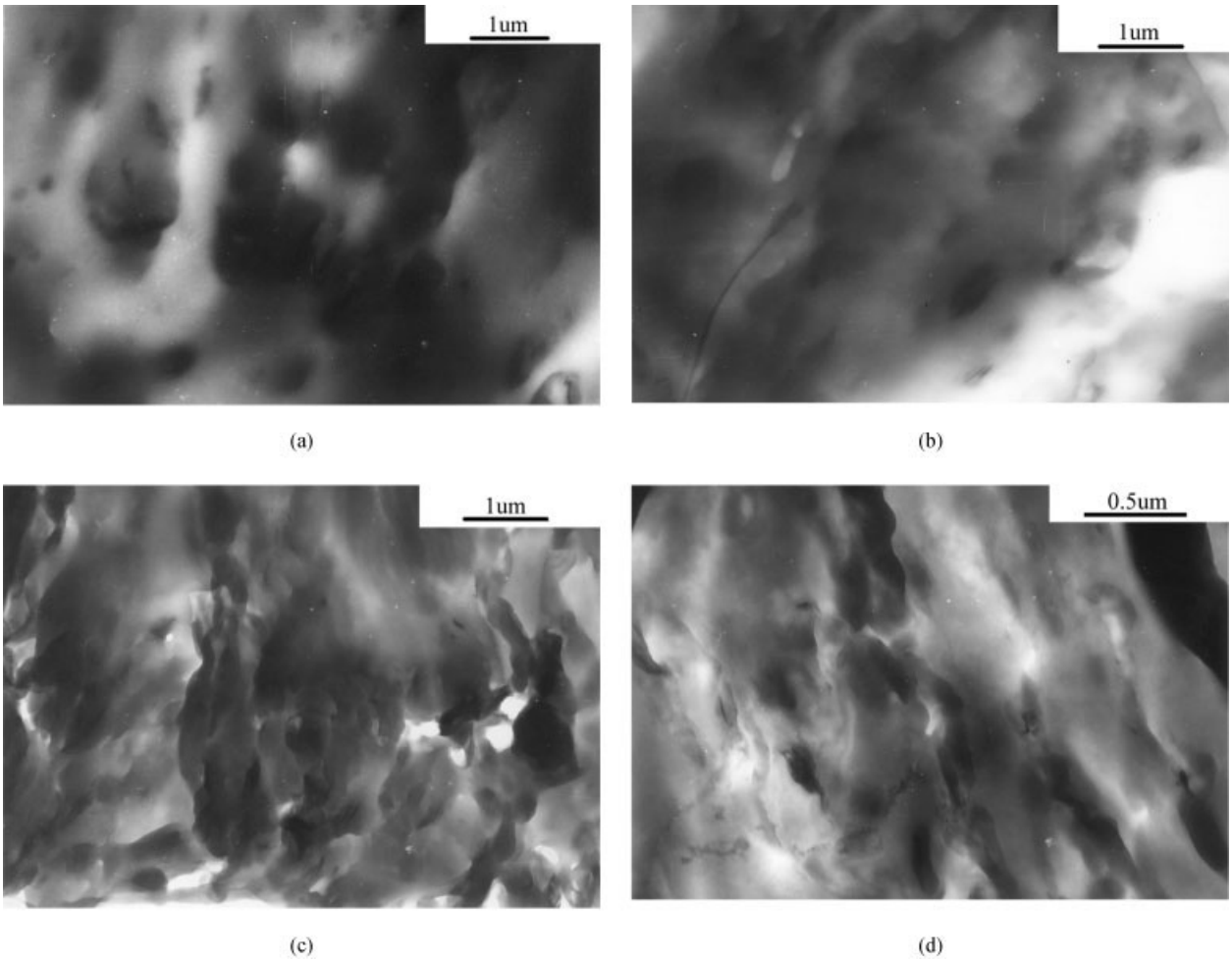

Figure 9 TEM images of (a) B1, (b) B2, (c) B3, and (d) B4.

image of B2 in Figure 9(b) indicates the increase of ABS domains size and a fine dispersion of ABS in the PBT matrix, and the clay layers staying in the PBT phase, consistent with the XRD analysis. Figure 9(c) presents the TEM micrograph of B3, which shows that the borderlines between the two phases are ambiguous and the clay layers disperse in both of PBT and ABS phases, but mostly in the PBT phase. The morphology change may be caused by the reversion of continuous phase and the lower melt viscosity of PBT than that of ABS. In ABS/OMT nanocomposites, the continuous phase is ABS, but ABS changes to the dispersed phase in B3. So the clay layers may rearrange and migrate to the low viscosity phase in B3. In B4 [Fig. 9(d)], irregular ABS domains nonuniformly distributed in the PBT matrix and most of the OMT dispersed in PBT and near the interfacial area like B1. The HREM images in Figure 10 indicate that the OMT was intercalated in sample B1, B2, B4 and partially exfoliated and partially intercalated in Sample B3, which is in agreement with the results of XRD.

Crystallization behavior of PBT in the compatibilized PBT and ABS alloys/OMT nanocomposites

PBT is a semicrystalline polymer with a high rate of crystallization while ABS is an amorphous polymer. However, the presence of ABS in blends with PBT has been shown to affect the crystallization behavior of PBT.[15,22] In PBT/clay nanocomposites, the effect of clay on the crystallization of PBT has attracted great interest.[29–31] In this study, mutual effect of ABS and OMT on the crystallization of PBT in the compatibilized PBT and ABS alloys/OMT nanocomposites were characterized by wide angle XRD. We found that the mixing sequences affect the crystalline microstructure of PBT in the compatibilized PBT and ABS alloys/OMT nanocomposites.

The XRD patterns of the neat PBT and its nanocomposites are presented in Figures 11–13. All XRD results show that although in the neat PBT and its blends there mainly exits the only α form (which is the stable crystalline form under relaxation of stress[35]), the rela-

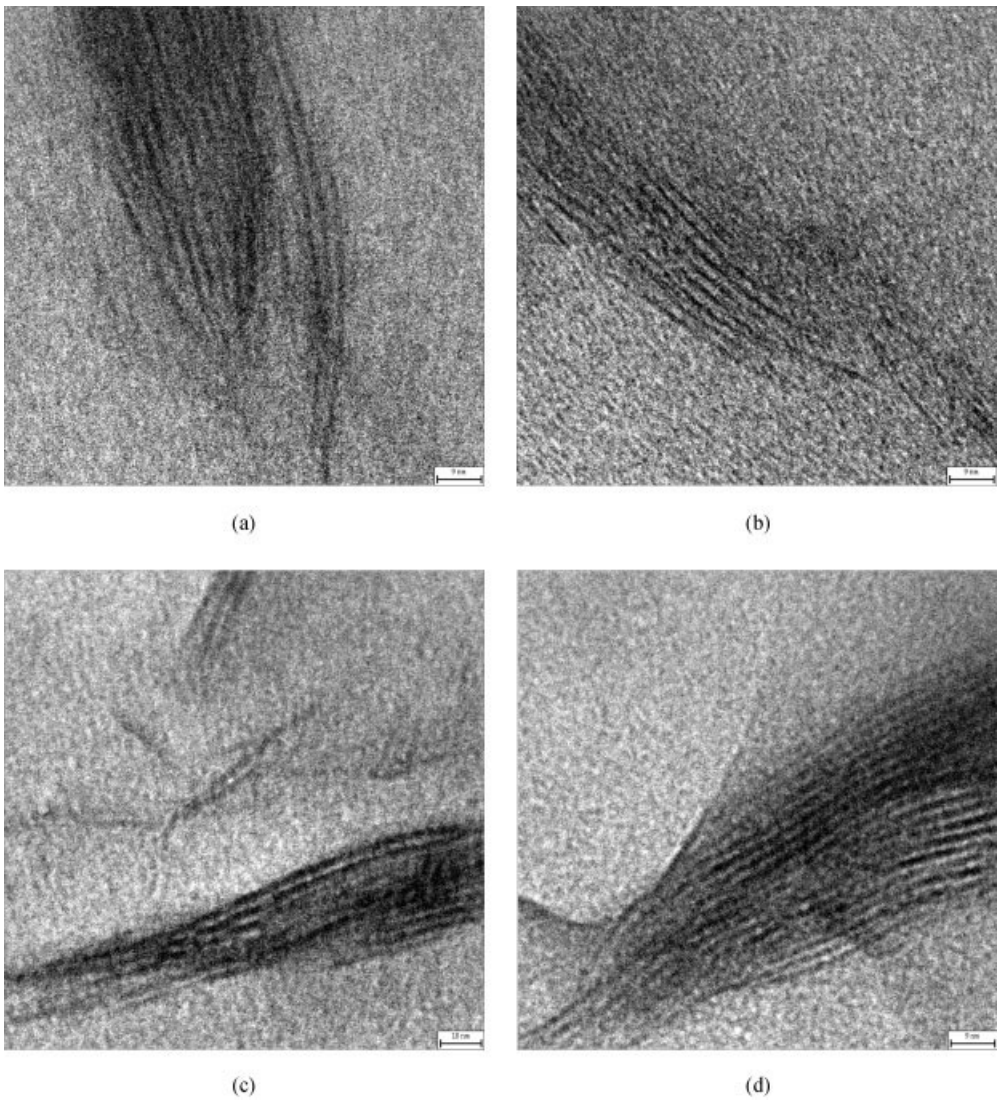

Figure 10 HREM images of (a) B1, (b) B2, (c) B3, and (d) B4.

tive intensity of the two peaks at 17.3° and 23.5° is different, which indicates the change in the crystal growing direction. It has been shown that these two peaks, respectively, represent diffractions of the (010) and (100) planes of PBT.[35] In PBT crystallites, there are the two types of spherulitic morphologies derived from different preferred radial orientations: in the "normal" spherulites the [$\bar{2}$10]* direction is parallel to the radial direction, whereas in the "abnormal" ones the [$\bar{1}$11]* direction is radial.[36,37] In the normal spherulites, the intensity of the (100) peak is higher than that of the (010) one. But the intensity of the (100) peak is lower than that of the (010) one in the abnormal spherulites.

For the neat PBT [Fig. 11(a)], the intensity of the (100) peak is higher than that of the (010) one, indicating the formation of normal spherulites. Figure 11 also shows the XRD patterns of B1 and B3. The intensity order of the two peaks kept unvaried like the neat

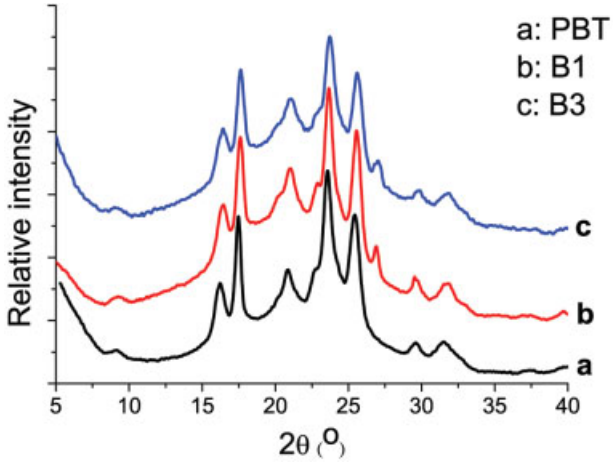

Figure 11 XRD patterns of (a) PBT, (b) B1, and (c) B3. [Color figure can be viewed in the online issue, which is available at www.interscience.wiley.com.]

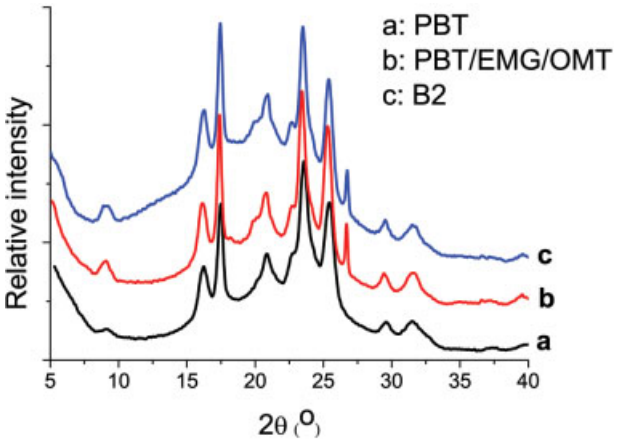

Figure 12 XRD patterns of (a) PBT, (b) the PBT/EMG/OMT nanocomposite, and (c) B2. [Color figure can be viewed in the online issue, which is available at www.interscience.wiley.com.]

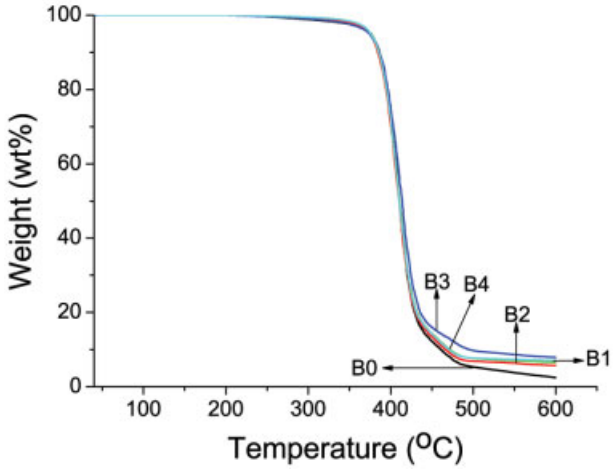

Figure 14 TG curves of B0, B1, B2, B3, and B4. [Color figure can be viewed in the online issue, which is available at www.interscience.wiley.com.]

PBT. The resemblance between B1 and B3 is that ABS and OMT were added into PBT matrix at the same time regardless of the mixing procedures. It shows that ABS and OMT added together do not change the crystal growing direction of PBT compared with pure one. However, when ABS and OMT were added not at the same time in B2 and B4, these show unique results. Figure 12(b) shows the normal spherulites in the PBT/EMG/OMT nanocomposites. After ABS were melt mixed with it in a second step, the relative intensities of the both peaks reversed in B2 [Fig. 12(c)]. The different phenomenon exits in B4. Figure 13 shows that the PBT/EMG/ABS blend formed abnormal spherulites while B4 formed normal ones after adding OMT. The presence of ABS changed the crystal growing direction and induced the formation of abnormal spherulites, (as shown in Ref. 22). In polymer/clay nanocomposites, the clay particles normally provided the additional heterogeneous nucleation sites to improve the crystallinity and did not change the crystal growing direction.[38] Our experiments suggest the latter additive determines whether it changes the crystal growing direction or not. It should be mentioned that in the nanocomposites including B1–B4 and PBT/EMG/OMT [Figs. 11(b,c); 12(b,c); 13(c)], the narrow diffraction peak near 26.7° belongs to the (100) plane of intergrowth α-SiO_2 in OMT, which keeps unvaried during the melt mixing.

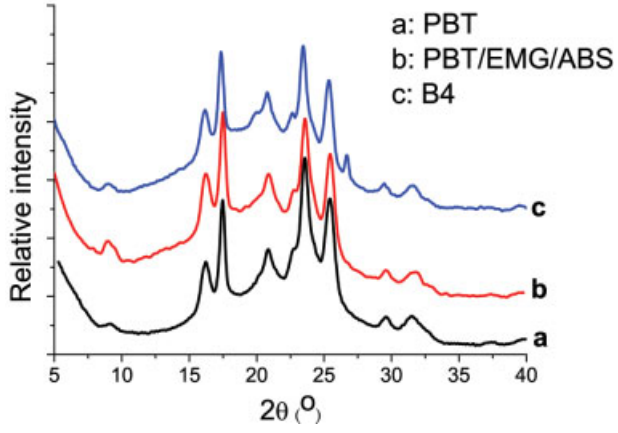

Figure 13 XRD patterns of (a) PBT, (b) the PBT/EMG/ABS blend, and (c) B4. [Color figure can be viewed in the online issue, which is available at www.interscience.wiley.com.]

Thermal properties of the compatibilized PBT and ABS alloys/OMT nanocomposites

Thermal stability is an important property for which the nanocomposites morphology plays an important role. The thermal properties of B0 and the compatibilized PBT and ABS alloys/OMT nanocomposites prepared by different mixing sequences were analyzed by thermogravimetric analysis (TGA). The TG curves are shown in Figure 14. An indistinct two-step thermal decomposition behavior is shown for all samples, where the decomposition of the first step is predominant. It may be attributed to the superposition of PBT and ABS degradations. The 3 wt % weight loss temperature ($T_{3\%}$), the maximum decomposition temperature of the first step (T_{max}) and char residue at 600°C are listed in Table II. It is obvious that the thermal stabilities of the compatibilized PBT and ABS alloys/OMT nanocomposites are enhanced compared with that of B0 and the order of mixing influences the thermal stabilities. The improvement of the thermal stability of the nanocomposites is likely to be due to an ablative reassembling of the reticular layers of the clay which may occur on the surface of the nanocomposites creating a physical protective barrier on the surface of the material and, on the other hand, volatilization

TABLE II
The TGA Data of the Compatibilized PBT/ABS/OMT Nanocomposites

Sample	$T_{3\%}$ (°C)	T_{max} (°C)[a]	Residue at 600°C (wt %)
B0	361.50	408.18	2.46
B1	366.60	408.74	4.17[b]
B2	365.40	408.65	3.34[b]
B3	359.60	411.83	5.56[b]
B4	367.35	409.05	4.70[b]

[a] Form DTG.
[b] The char for OMT at 600°C has already been subtracted.

might also be delayed by the labyrinth effect of the silicate layers dispersed in the nanocomposites.[39] From Table II, it shows that in the initial stage, the degradation of B2 and B3 are slightly quicker than that of B1 and B4, especially $T_{3\%}$ of B3 is smaller than that of B0. It may be due to the difference of processing history. As shown in the experimental section, OMT experienced both of the two steps mixing for B2 and B3 while it was used in one step blending for B1 and B4. So more amounts of organic modifiers in OMT for B2 and B3 were released, which may accelerate the decomposition of polymer chains.[30,40] Among the four compatibilized PBT and ABS alloys/OMT nanocomposites, T_{max} value of B3 is the biggest. It may be attributed to the partially exfoliated and partially intercalated morphology in B3, which made the clay layers disperse more uniform and induced the barrier effect more effective.

Effect of addition of ABS and OMT into PBT through different order of mixing on the thermal properties of the nanocomposites was studied by DSC. Figures 15 and 16, respectively, present the DSC curves of neat PBT and B0–B4 recorded during the heating steps and cooling steps (20°C/min). The results are summarized in Table III. As shown in Table III and Figure 15, T_g belonging to styrene–acrylonitrile phase of ABS in B0 is 108.07°C. And all T_g in the compatibilized PBT and ABS alloys/OMT nanocomposites (B1–B4) increase. It is attributed to the effect of OMT on the polymer chains.[31] When heating at the rate of 20°C/min (Fig. 15), multiple melting endothermic peaks are observed in all samples as before.[41] Elaborate studies have shown that the phenomenon is due to the melting–recrystallization process during heating. In neat PBT, the crystallinity is 28.55% while that in B0 is 28.10%. It shows that ABS depresses the PBT crystalline. However, the crystallinity of PBT in the nanocomposites (B1–B4) all are higher than that of neat PBT and B0, indicating that OMT promotes the crystallization of PBT and the effect of OMT is higher than that of ABS. The difference between B1 and B4 may be due to the morphology of nanocomposites.

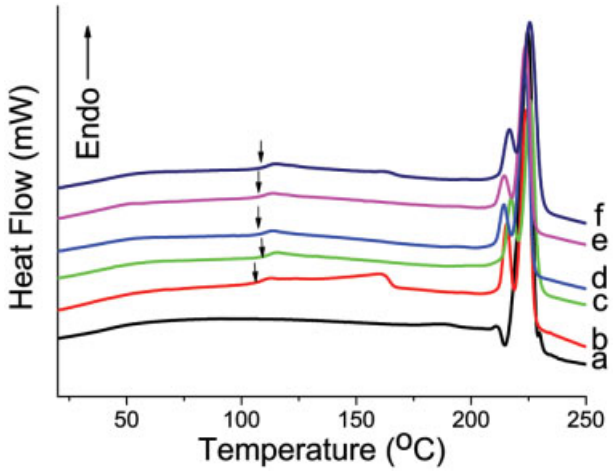

Figure 15 DSC thermograms recorded during the heating steps (20°C/min) for (a) PBT, (b) B0, (c) B1, (d) B2, (e) B3, and (f) B4. Arrows indicate the position of the glass transition temperatures, T_gs. [Color figure can be viewed in the online issue, which is available at www.interscience.wiley.com.]

CONCLUSIONS

The PBT and ABS alloys/OMT nanocomposites using EMG including GMA repeat units as the reactive compatibilizer were prepared by melt intercalation method. The results characterized by SEM, XRD, TEM, and HREM showed that order of mixing has influence on the dispersion state of OMT and the morphology of the PBT/ABS alloys. The crystallization behavior studies indicated that the preferential crystal growing direction of PBT was determined by the last additive of ABS and OMT. It may be attributed to the antagonistic effect of ABS and OMT. TGA and DSC experiments showed order of mixing affect the thermal

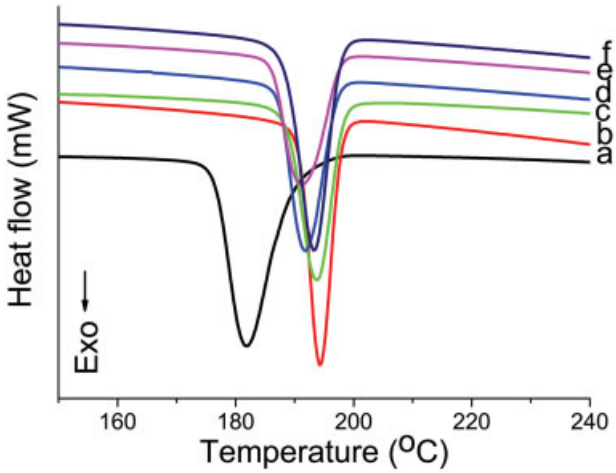

Figure 16 DSC thermograms recorded during the cooling steps (20°C/min) for (a) PBT, (b) B0, (c) B1, (d) B2, (e) B3, and (f) B4. [Color figure can be viewed in the online issue, which is available at www.interscience.wiley.com.]

TABLE III
DSC Results of the Compatibilized PBT/ABS/OMT Nanocomposites

Sample	T_g (°C)	T_{m1} (°C)	T_{m2} (°C)	ΔH_m (J/g)	Crystallinity of PBT (%)[a]	T_c (°C)	ΔH_c (J/g)
PBT	—	211.31	224.68	40.53	28.55	181.85	48.10
B0	108.07	215.45	223.98	25.94	28.10	194.20	29.42
B1	111.16	217.29	225.82	27.20	30.90	193.87	28.23
B2	109.87	214.11	223.47	26.59	30.20	191.84	29.69
B3	109.27	214.28	223.64	26.15	29.70	191.18	28.99
B4	110.80	216.45	225.64	27.32	31.03	193.19	29.45

[a] Crystallinity of PBT (%) = $\Delta H_m \times 100/(142 \times \%m_{PBT})$

properties of the compatibilized PBT and ABS alloys/OMT nanocomposites. It may be owing to processing history and the formed microstructure.

This work was financially supported by the National Natural Science Foundation of China (No. 50323005) and (No. 50476026), and the Doctor Foundation of AIAI.

References

1. Cruz, C. A.; Havriliak, S. J.; Slavin, S. Proceedings of Additives' 95, Executive Conference Management, Clearwater Beach, FL, February 22–24, 1995.
2. Brady, A. J.; Keskkula, H.; Paul, D. R. Polymer 1994, 35, 3665.
3. Holsti-Miettinen, R. M.; Heino, M. T.; Seppala, J. V. J Appl Polym Sci 1995, 57, 573.
4. Cecere, A.; Greco, R.; Ragosta, G.; Carinzi, G. Polymer 1990, 31, 1239.
5. Kim, S. J.; Shin, B. S.; Hong, J. L.; Cho, W. J.; Ha, C. S. Polymer 2001, 42, 4073.
6. Kim, S. J.; Kang, C. J.; Chowdhury, S. R.; Cho, W. J.; Ha, C. S. J Appl Polym Sci 2003, 89, 1305.
7. Binsack, R.; Rempel, D.; Humme, G.; Ott, K. H. (Bayer), U.S. Pat. 4,292,233 (1981).
8. Binsack, R.; Rempel, D.; Lindner, C.; Morbitzer, L. (Bayer), U.S. Pat. 4,535,124 (1985).
9. Wang, I. C. W. (General Electric), US Pat. 4,753,986, 1988.
10. Hourston, D. J.; Lane, S. In Rubber Toughened Engineering Plastics; Collyer, A. A., Ed.; Chapman and Hall: London, 1994; p 243.
11. Lee, P. C.; Kuo, W. F.; Chang, F. C. Polymer 1994, 35, 5641.
12. Ultracki, L. A. Polym Eng Sci 1995, 35, 2.
13. Benson, C. M.; Burford, R. P. J Mater Sci 1995, 30, 573.
14. Van Berkel, R. W. M.; Van Hartingsveldt, E. A. A.; Van der Sluijs, C. L. In Handbook of Thermoplastics; Olabisi, O., Ed.; Marcel Dekker: New York, 1997; p 465.
15. Hage, E.; Hale, W.; Keskkula, H.; Paul, D. R. Polymer 1997, 38, 3237.
16. Basu, D.; Banerjee, A. J Appl Polym Sci 1997, 64, 1485.
17. Hale, W.; Keskkula, H.; Paul, D. R. Polymer 1999, 40, 365.
18. Hale, W.; Keskkula, H.; Paul, D. R. Polymer 1999, 40, 3665.
19. Hale, W.; Pessan, L. A.; Keskkula, H.; Paul, D. R. Polymer 1999, 40, 4237.
20. Hale, W.; Lee, J. H.; Keskkula, H; Paul, D. R. Polymer 1999, 40, 3621.
21. Hale, W.; Keskkula, H.; Paul, D. R. Polymer 1999, 40, 3353.
22. Hage, E.; Ferreira, L. A. S.; Manrich, S.; Pessan, L. A. J Appl Polym Sci 1999, 71, 423.
23. Mantovani, G. L.; Canto, L. B.; Hage, E.; Pessan, L. A. Macromol Symp 2001, 176, 167.
24. Sun, S. L.; Xu, X. Y.; Yang, H. D.; Zhang, H. X. Polymer 2005, 46, 7632.
25. Alexandre, M.; Dubois, P. Mater Sci Eng 2000, 28, 1.
26. Gilman, J. W.; Kashiwagi, T.; Lichtenhan, J. D. SAMPE J 1997, 33, 40.
27. Li, X.; Kang, T.; Cho, W. J.; Lee, J. K; Ha, C. S. Macromol Rapid Commun 2001, 22, 1306.
28. Li, X.; Park, H. M.; Lee, J. O.; Ha, C. S. Polym Eng Sci 2002, 42, 2156.
29. Chisholm, B. J.; Moore, R. B; et al. Macromolecules 2002, 35, 5508.
30. Xiao, J. F.; Hu, Y.; Wang, Z. Z.; Tong, Y.; Chen, Z. Y.; Fan, W. C. Eur Polym J 2005, 41, 1030.
31. Chang, J. H.; An, Y. U.; Kim, S. J; Im, S. Polymer 2003, 44, 5655.
32. Tripathy, A. R.; Burgaz, E.; Kukureka, S. N.; Macknight, W. J. Macromolecules 2003, 36, 8593.
33. Illers, K. H. Colloid Polym Sci 1980, 258, 117.
34. Ray, S. S.; Pouliot, S.; Bousmina, M.; Utracki, L. A. Polymer 2004, 45, 8403.
35. Yokouchi, M.; Sakakibara, Y.; Chatani, Y.; Tadoboro, H.; Tanaka, T.; Yoda, K. Macromolecules 1976, 9, 266.
36. Stein, R. S.; Misra, A. J Polym Sci Polym Phys Ed 1980, 18, 327.
37. Roche, E. J.; Stein, R. S.; Thomas, E. L. J Polym Sci Polym Phys Ed 1980, 18, 1145.
38. Ke, Y.; Long, C.; Qi, Z. J Appl Polym Sci 1999, 71, 1139.
39. Gilman, J. W.; Kashivagi, T. C. L.; Giannelis, E. P.; Manias, E.; Lomakin, S.; Lichtenhan, J. D.; Jones, P. In Fire Retardancy of Polymer; Le Bras, M., Camino, G., Bourbigot, S., Delobel, R., Eds.; The Royal Society of Chemistry: Cambridge, 1998.
40. Xie, W.; Gao, Z.; Pan, W. P.; Hunter, D.; Singh, A.; Vaia, R. A. Chem Mater 2001, 13, 2979.
41. Nichols, M. E.; Robertson, E. E. J Polym Sci Part B: Polym Phys 1992, 30, 755.